Development of Infrared Scene Projectors
for Testing Fire-Fighter Cameras

Jorge E. Neira[a], Joseph P. Rice[a], Francine K. Amon[b]

[a]Optical Technology Division, Physics Laboratory
[b]Fire Research Division, Building and Fire Research Laboratory
National Institute of Standards and Technology, Gaithersburg, MD 20899

ABSTRACT

We have developed two types of infrared scene projectors for hardware-in-the-loop testing of thermal imaging cameras such as those used by fire-fighters. In one, direct projection, images are projected directly into the camera. In the other, indirect projection, images are projected onto a diffuse screen, which is then viewed by the camera. Both projectors use a digital micromirror array as the spatial light modulator, in the form of a Micromirror Array Projection System (MAPS) engine having resolution of 800 x 600 with mirrors on a 17 micrometer pitch, aluminum-coated mirrors, and a ZnSe protective window. Fire-fighter cameras are often based upon uncooled microbolometer arrays and typically have resolutions of 320 x 240 or lower. For direct projection, we use an argon-arc source, which provides spectral radiance equivalent to a 10,000 Kelvin blackbody over the 7 micrometer to 14 micrometer wavelength range, to illuminate the micromirror array. For indirect projection, an expanded 4 watt CO_2 laser beam at a wavelength of 10.6 micrometers illuminates the micromirror array and the scene formed by the first-order diffracted light from the array is projected onto a diffuse aluminum screen. In both projectors, a well-calibrated reference camera is used to provide non-uniformity correction and brightness calibration of the projected scenes, and the fire-fighter cameras alternately view the same scenes. In this paper, we compare the two methods for this application and report on our quantitative results. Indirect projection has an advantage of being able to more easily fill the wide field of view of the fire-fighter cameras, which typically is about 50 degrees. Direct projection more efficiently utilizes the available light, which will become important in emerging multispectral and hyperspectral applications.

Keywords: Infrared, projector, camera, fire-fighter, thermal, imaging, diffraction, micromirrors, HWIL

1. INTRODUCTION

Infrared technology for fire fighting applications has matured to the point that most first responder organizations either have purchased or are considering the purchase of one or more infrared thermal imaging cameras. Such cameras can provide first responders with critical information to size up a fire incident, track fire growth, and to locate victims, other first responders, and egress routes. For example, uncooled long-wavelength infrared (LWIR) cameras are capable of seeing humans through dense smoke under certain conditions. However, these devices represent a significant investment, typically on the order of $ 10,000 per camera, for first responders and there is currently little guidance on instrument performance beyond manufacturer literature and recommendations from other users.[1] These issues are further complicated because the demands placed on thermal-imaging cameras depend on the specific application. The end users may have very different ideas about which imaging properties are most important: sharp image contrast may be sufficient for some fire fighting applications, such as finding the source of a fire, but high thermal sensitivity may be required to locate a person or structural component when flames and water are in the imager's field of view. Currently, there are no standardized performance guidelines available to aid end users in making purchasing decisions.

Over the past several years, the Fire Research Division at the National Institute of Standards and Technology (NIST) has been conducting research on thermal imaging camera performance metrics and test methods with the overall objective of

Correspondence: joe.rice@nist.gov

providing science-based information to national standards developing organizations. The National Fire Protection Association (NFPA) is currently developing a standard on first responder thermal imaging cameras, draft NFPA 1801,[2] and the American Society of Testing and Materials (ASTM) is revising a test method on infrared detector sensitivity, ASTM E1543-00.[3] Both of these organizations are taking this work into consideration as they move through their standards developing processes.

Experimental research on testing thermal imaging cameras in the NIST Fire Research Division has so far been conducted in two main areas: room-sized live-fire testing and thermal-bar-based contrast transfer function testing. Live-fire testing is expensive and difficult to precisely repeat. Contrast transfer testing with thermal bars is limited in scope. Therefore, we have embarked on a third approach: use of an infrared scene projector to provide either realistic scenes to simulate live fires, or sinusoidal and bar patterns for modulation transfer function and contrast testing. When fully developed, we anticipate that this approach could provide a reproducible method of testing thermal imaging cameras with a wide scope of images and video clips.

Here we report our progress in using a Texas Instruments digital micromirror device (DMD) in the form of an Optical Sciences Corporation Micromirror Array Projection System (MAPS) engine as an infrared scene projector for this application.[*] Details of the MAPS as used with blackbody illumination have been described previously,[4-6] and some prior work using a MAPS engine with infrared laser illumination has been reported.[7,8] However, the wavelengths of interest for fire-fighter cameras approach the pixel size of the DMD, so diffraction effects are important. We sought a deeper understanding than available in these published references of how to optimize the projector with diffraction in mind, so our approach was to first characterize the MAPS DMD as diffraction grating using a CO_2 laser, as described in Section 2. Based on the insight obtained, we constructed two types of projectors, as described in Section 3. Finally, as described in Section 4, we began performing test of the modulation transfer function on these systems.

2. DMD DIFFRACTION CHARACTERIZATION

The MAPS DMD engine consists of an 800 x 600 array of micromirrors on a 17 μm pitch and (on/off) tilt angle of ±10 degrees about the micromirror diagonal. It has a ZnSe window with anti-reflection (AR) coatings optimized for the 3 μm to 12 μm spectral band, and the micromirrors are aluminum coated. In the unpowered state the mirrors are flat (0 degrees, nominally aligned with the DMD window). Since the size of each micro mirror is of the order of the wave length of our illumination source, the DMD will diffract most of the incoming light. To understand the basic mechanism in which the DMD could be used to project images in the 7 micrometer to 14 micrometer spectral range, a 4 Watt tunable CO_2 laser was used to illuminate the MAPS DMD normal to its window and the diffracted light was projected onto a beadblasted aluminum screen. Figure 1 depicts the experimental arrangement used for basic diffraction studies.

A laboratory-grade uncooled infrared camera was utilized for these experiments. It has a 320 x 240 microbolometer array sensitive in the 7 μm to 14.0 μm range, thermally stabilized at a temperature of 313 K, is equipped with a 50 mm focal length germanium lens. It provided a real time, 60 Hz, 12 bit data stream as a standard output format, with a variable integration time. The microbolometer camera was calibrated for radiance responsivity using an extended-area blackbody that overfilled its pupil. A thirteen point calibration that ranged in temperature from 283.15 K to 348.15 K in 5 K steps was performed with this blackbody. This calibration also served to provide a non-uniformity correction for the camera. The radiometric calibration and non-uniformity correction based on these measurements was then maintained by updates based on a single image of the blackbody at a known temperature (308.15 K) taken near the time of any subsequent measurements.

Multiple images were taken with the camera with the above configuration, all at a camera integration time of 41 ms. The first set of images was taken with all DMD mirrors "on" and then all DMD mirrors "off" as shown in Fig. 2 and Fig. 3, respectively. In these images the DMD housing, which can be seen faintly, obscures the central region of the screen along the optical axis, including some stray light from the DMD window that was seen when the camera was moved to avoid this obscuration. From this set of images, the measured screen-to-camera image magnification, and the distance between the DMD and the screen, the computed angle between the DMD normal and each of the spots seen in Fig. 2 and Fig. 3 and is $\beta = 38.2° \pm 1°$ (k=1).
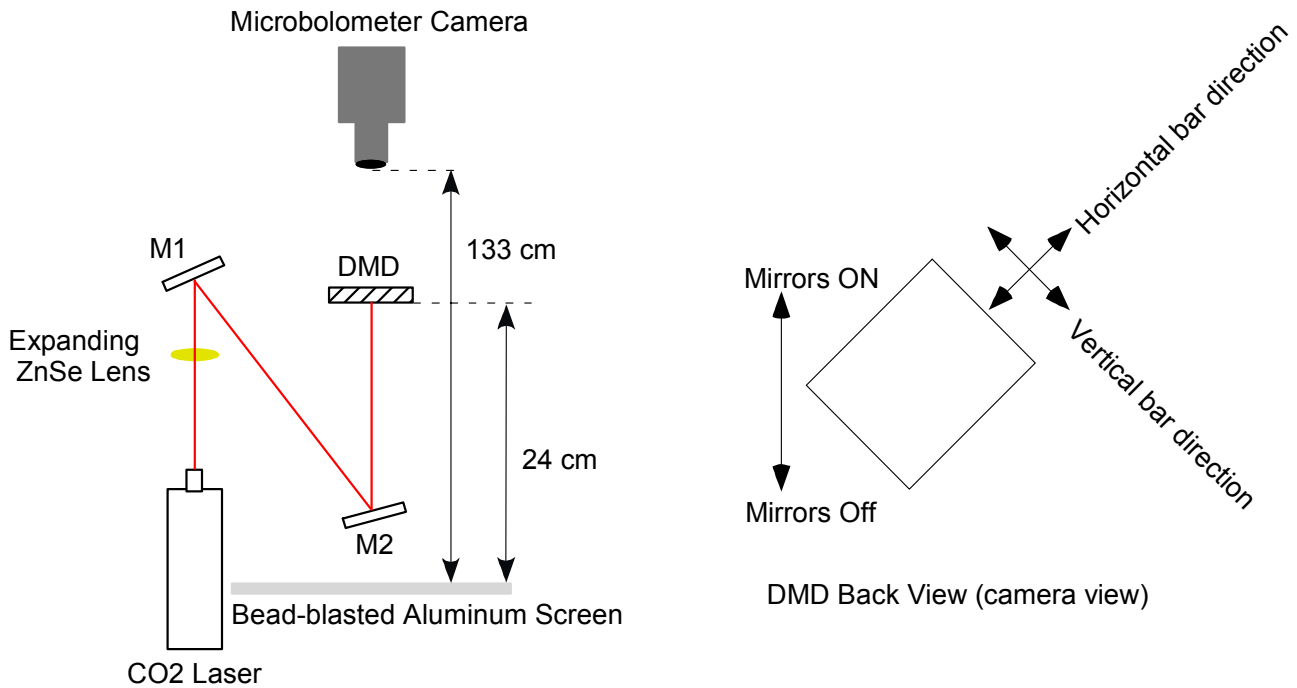
Figure 1. Experiment arrangement for DMD Characterization (not to scale).

We interpret the four bright rectangular "spots" seen in Fig. 2 and Fig. 3 as multiple images of the DMD array that arise from first order diffraction. The dimensions of each diffracted DMD image are actually slightly larger than the DMD itself, which is reasonable given the slight divergence of the laser beam. Following others,[9] we model the DMD as a double-ruled diffraction grating, where one axis of the grating is rotated 90 degrees about the DMD normal from the other, thereby providing two sets, $m = \pm 1$ and $n = \pm 1$, of first order diffraction spots, rotated by 90 degrees from each other. With the angle of incidence $\alpha = 0$ and the angle of diffraction β, the equation for a simple one-dimensional grating is

$$m\lambda = d \sin \beta \tag{1}$$

where d is the native groove spacing (17 μm for the DMD used here), λ is the wavelength (10.6 μm here), and m (or n for the orthogonal direction) is the diffraction order. From Eq. (1) the theoretical first order diffraction angle from this DMD is $\beta = 38.6°$, in close agreement with our experimentally measured value.

To gain some understanding of the relative intensity values for the diffracted spots in Fig. 2 and Fig. 3, it is useful to consider the first order blaze condition for a grating under normal incidence illumination,[10]

$$\lambda_B = d_B \sin 2\phi \tag{2}$$

where ϕ is the blaze angle of the facets and d_B is the periodic spacing between the blazed facets. For the DMD used here, $\phi = +10°$ for "on" micromirrors, $\phi = -10°$ for "off" micromirrors, where the axis for these angles is the diagonal of the micromirrors as shown in Fig. 4. The diagonal of the micromirrors corresponds to the horizontal axis in Fig. 2 and Fig. 3 since the DMD was rotated about its normal by 45° relative to the camera. From Fig. 4 the DMD with all micromirrors "on" (or all "off") can be thought of as a blazed grating with sawtooth-shaped grooves having blazed facet

periodicity of $d_B = \sqrt{2}\, d = 24$ μm along the vertical direction of the camera images (with the particular orientation that we used). Then, from Eq. (2) the blaze wavelength, corresponding to maximum efficiency, is $\lambda_B = 8.2$ μm. The region of efficient diffraction for a blazed grating typically extends from about 2/3 to 3/2 of λ_B,[11] which encompasses the test wavelength ($\lambda = 10.6$ μm) used here. Thus the angle of the facets and their direction influences the relative intensity of the diffracted intensity because we are operating near the blaze condition. We suggest that this explains why the diffracted radiance for the two spots in the "on" direction is greater than that of the two spots in the "off" direction when all mirrors are "on" (Fig. 2), and why the same thing happens, but in the opposite direction, when all mirrors are "off" (Fig. 3). A simple contrast ratio was calculated by integrating the radiance of one of the diffraction orders over a region and dividing the "on" state values by the "off" state value after subtracting the radiance background. The best contrast ratio computed in this manner was found to be 2.6 with the $m = +1$ diffraction order.
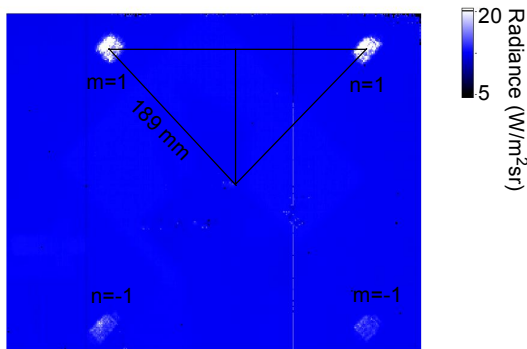

Figure 2. Image projected on the screen with all mirrors on. The distance on the screen between the *m*=1 spot and the optical axis is 189 mm, as indicated. The DMD housing, the back of which appears faintly as a diagonally-oriented rectangle in this image, obstructs the view of the region near the optical axis.
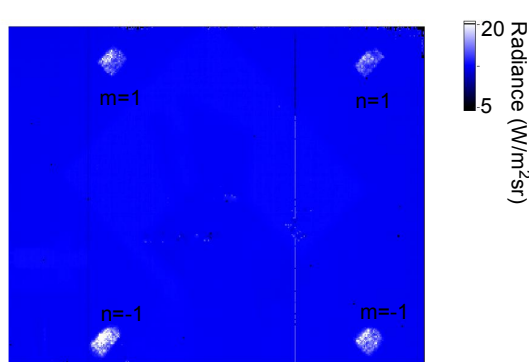
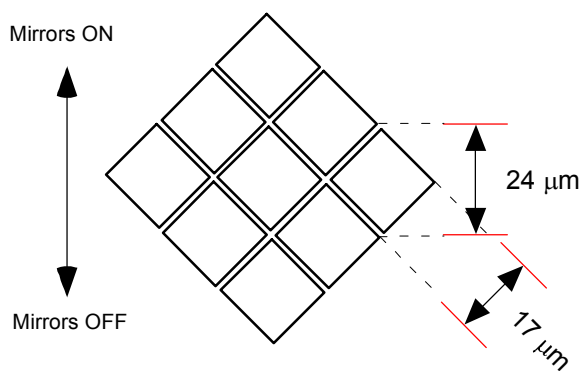**Figure 3.** Same as Fig. 2, except with all mirrors off.

Figure 4. The DMD can be thought of as two sets of orthogonally-ruled gratings having a pitch of 17 μm. Each "on" mirror is tilted about its horizontal diagonal (as oriented in this drawing) such that normally-incident rays are reflected upwards towards the screen. Each "off" mirror is tilted about the horizontal diagonal such that normally-incident rays are reflected downwards towards the screen. The blazed facet periodicity in the plane of incidence/reflectance is 24 μm.

A number of images were acquired with a series of bar patterns displayed on the MAPS DMD. For the first set of tests, the bars were parallel to the horizontal axis of the DMD, and each bar cycle consisted of number of "on" mirrors and an equal number of "off" mirrors. Fig. 5 and Fig. 6 show the radiance-calibrated images for 100 mirrors/cycle and 10 mirrors/cycle on the DMD, respectively. From Fig. 6 one can begin to see multiple spots, perhaps arising from multiple slit diffraction effects from the bar patterns. By 2 mirrors/cycle, the maximum possible, a new diffraction pattern appeared on the screen as shown in Fig. 7 for the horizontal bar pattern, and in Fig. 8 for the vertical bar pattern. Here the diffraction angle in the direction perpendicular to the bar pattern (diagonal in the camera images) was measured to be $\beta_{bar} = 18.5° \pm 1°$ (k=1), as listed in Table 1. This makes sense from Eq. (1) when the groove spacing is the distance d_{bar} between neighboring bars, which is $2d = 34$ μm for 2 mirrors/cycle for the MAPS DMD used here, giving $\beta_{bar} = 18.2°$. Repeating the test at a different wavelength of the CO_2 laser, $\lambda = 9.5$ μm, gave $\beta_{bar} = 16.5° \pm 1°$ (k=1) as listed in Table 1, which again agrees with the Eq. (1) prediction of $\beta_{bar} = 16.2°$ at this wavelength. A simple contrast ratio was computed with this 2 mirrors/cycle diffraction pattern to be approximately 40, far surpassing that obtained above from the all-on pattern. By using this diffraction effect and the efficiency offered by operating near the blaze wavelength, we increase the efficiency of the DMD and also its contrast ratio in the projection schemes described below.
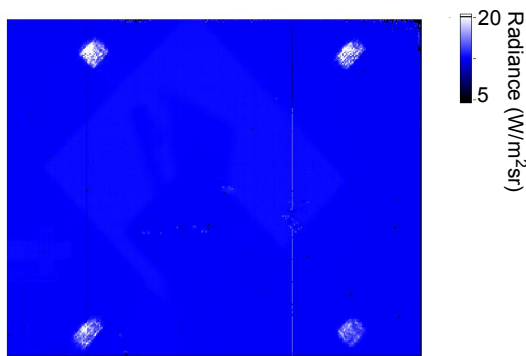

Figure 5. Same as Fig. 2, except with the DMD displaying a horizontal bar pattern having 100 mirrors/cycle.
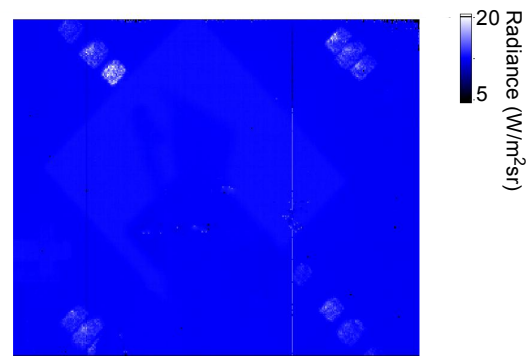

Figure 6. Same as Fig. 5, except with the DMD displaying a horizontal bar pattern having 10 mirrors/cycle.
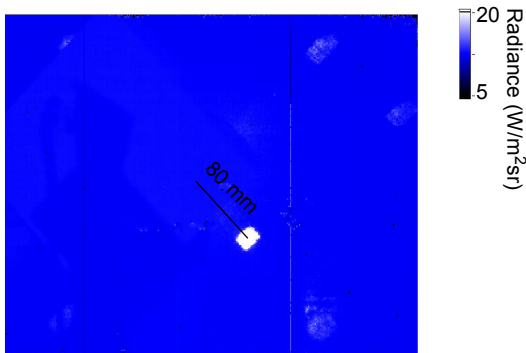

Figure 7. Same as Fig. 2, except with the DMD displaying a horizontal bar pattern having 2 mirrors/cycle. The distance on the screen from the optical axis to the bright diffraction spot was 80 mm, as indicated.
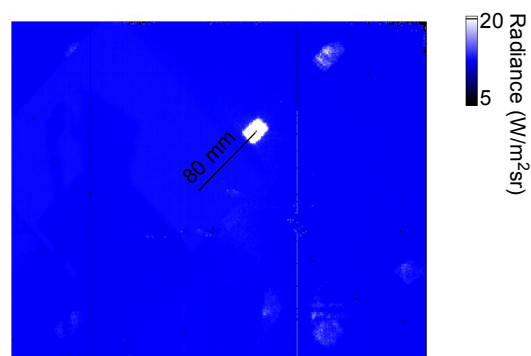

Figure 8. Same as Fig. 7, except with the DMD displaying a vertical bar pattern having 2 mirrors/cycle. The distance on the screen from the optical axis to the bright diffraction spot was 80 mm, as indicated.

Table 1. Diffraction experiment results for horizontal bars. D is the distance from the DMD to the projection screen, α is the incidence illumination angle on the DMD, β_{bar} is the diffraction angle measured to the bright spot on Fig. 7 when a 2 mirror/cycle bar pattern was displayed on the DMD, and λ is the wavelength of the CO_2 laser. These angular measurements are with respect to the vector normal to the DMD window. Angular measurements were made with an uncertainty of $\pm1°$ (k=1), while distance measurements were made with an uncertainty of ±3 mm (k=1).

λ (μm)	β_{bar} (degrees)	α (degrees)	D (mm)
10.6	18.5 ± 1	0	240
9.5	16.5 ± 1	0	240

3. DEVELOPMENT OF AN INFRARED SCENE PROJECTOR

Two different types of arrangement were tested for use as projector systems. One is based on a CO_2 laser and uses indirect projection, while the other is based on an argon arc source and uses direct projection. Fig. 9a depicts the complete CO_2 laser projection system. A CO_2 laser, with 3.5 Watt nominal output power at 10.6 microns was used as the illumination source. A dithering mirror was used in to homogenize the expanded CO_2 laser beam. ZnSe AR-coated projection optics were used to project the image displayed on the DMD onto a rotating aluminum-painted screen. The rotation very effectively eliminated laser spackle, which otherwise significantly deteriorated the projected image.

Fig. 9b depicts the setup for direct projection. A collimated beam from an argon arc source, having a radiance output over the 7 μm to 11 μm spectral band comparable to a 10,000 K blackbody,[12] was used as the illumination source through mirrors M1, M2, and M3. The angle of incidence was varied. A single ZnSe AR-coated projection lens was used to optically couple to the camera, and mirror M4 was used to direct the beam flooding the off-state DMD mirrors towards a liquid nitrogen (LN_2) cold source to reduce the radiance background diffracting from the DMD.

a)   b)
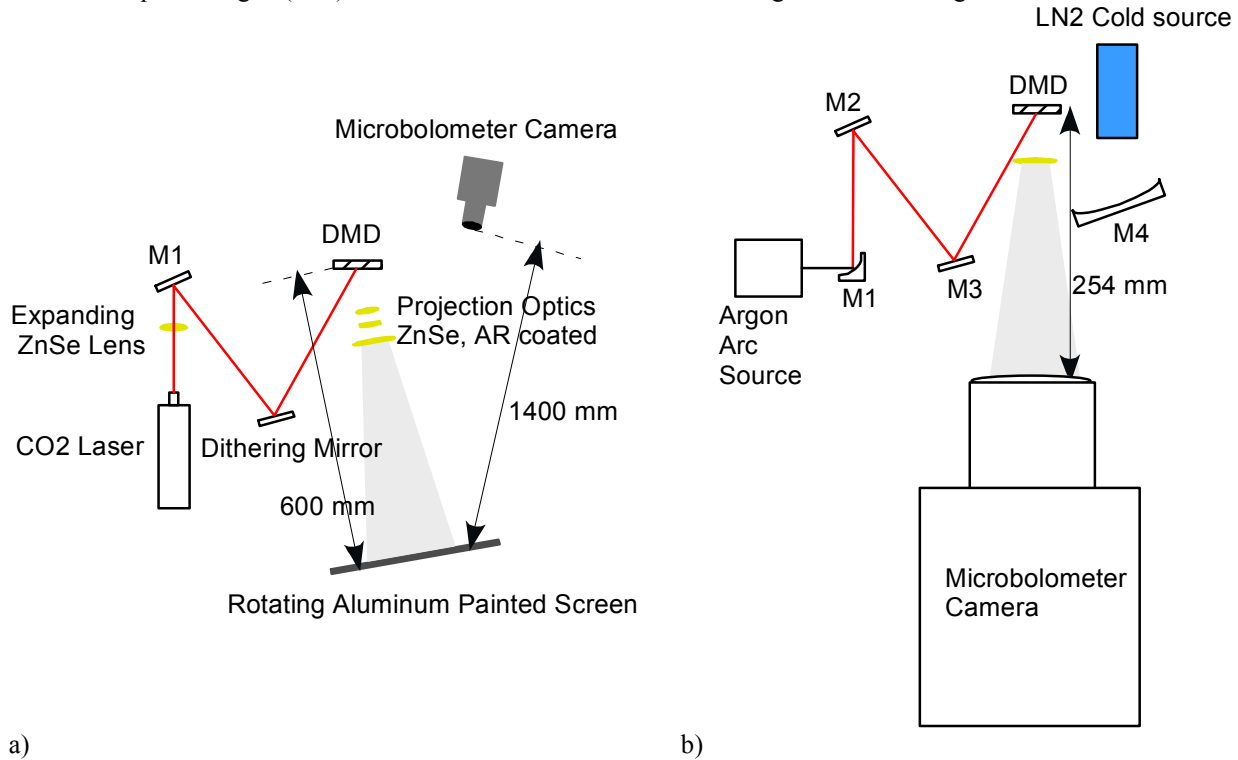
Figure 9. Schematic arrangement for (a) indirect projection and (b) direct projection. Top views. Not to scale.

Motivated by the 2 mirrors/cycle diffraction result described above, a "micro-slit" projection scheme was developed. Binary as well as gray scale imagery was projected with the MAPS engine using this scheme. A single micro-slit pixel is defined to consist of 1 horizontal by 2 vertical DMD mirrors. Within this 1×2 pixel one of the micromirrors is always in "off" state, and the other is in either the "on" or the "off" state for binary projection, and was set to an integer value from 0 to 255 in the case of 8 bit gray-scale projection using the MAPS pulse-width-modulation algorithm. The image pre-processing works as follows. The input image frame is initially re-scaled to a resolution of 800 horizontal (H) by 600 vertical (V) in order to fit the MAPS DMD resolution. Then the image is further re-scaled in the vertical direction to get an 800 H by 300 V resolution image. Finally each pixel in the image is converted to a micro-slit pixel. This amounts to inserting an "off" state row in every other display row, so the resolution of the final image to display on the DMD is 800 H by 600 V, as required. Here and throughout this paper we use the term resolution to refer only to the number of pixels in the image data array, not to the actual optical resolution achieved upon projection.

Figure 10 shows an example of the micro-slit image process as applied to a real scene. Fig. 10a is the input image before conversion after being rescaled to fit the DMD (800 × 600). Fig. 10b is the image after being converted to micro-slit format. Figure 10c is magnification of the upper right portion of Fig. 10b, near the letter "T". The image as projected by the system shown in Fig. 9b and captured by the laboratory microbolometer infrared camera is shown in Fig. 10d. Because of the non-optimized magnification of the projection optics used here, the DMD is only covering 25% of the field of view of the camera and therefore the resolution of the image is only 80X60, giving rise to the pixelization that dominates this image.
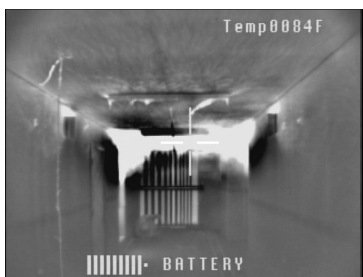

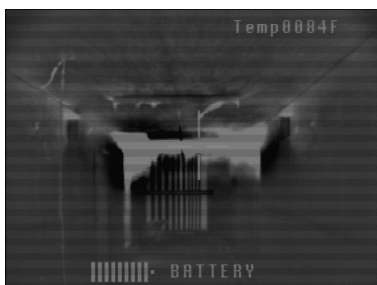**Figure 10a.** Original image at 800 × 600 resolution.
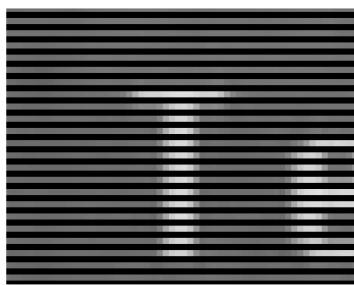

Figure 10b. Micro-slit format.

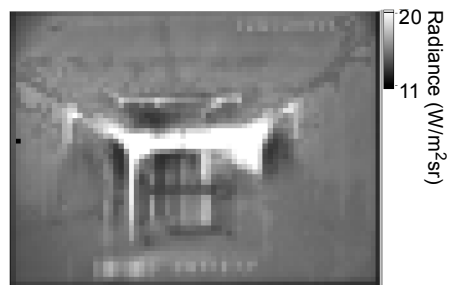**Figure 10c.** Magnified part of Fig. 10b.

Figure 10d. Projected, then captured at 80 × 60 resolution.

Figure 10e. Micro-checker format.

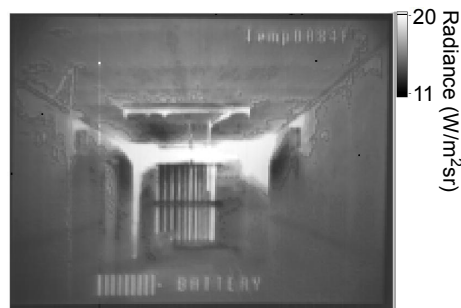**Figure 10f.** Magnified part of Fig. 10e.

Figure 10g. Projected, then captured at 160 × 120 resolution.

A second scheme was studied which seems to diffract more energy useful for projection. This "micro-checker" scheme works the same as the micro-slit scheme with the exception that each micro-checker pixel consists of a quad of 2×2 DMD mirrors. Within the quad one diagonal pair of mirrors was always in the on-state, and the other pair encoded the 8-bit gray scale in the usual manner. Fig. 10e through 10g are the same sequence as explained above, but using the micro-checker scheme. Note that Fig. 10e looks like the negative of the input image since here we used "on" state DMD mirrors to represent the off condition. The projected image as captured by the microbolometer camera is shown in Fig. 10g. In this case, the DMD was covering 50% of the field of view of the camera and therefore the resolution of the image was 160×120, so pixelization was not as evident as above. Recall that the microbolometer camera resolution was 320×240.

The original scene used in this example is one frame from a video clip of a realistic scene used for testing fire-fighter cameras during live-fire testing by the Fire Research Division at NIST. Smoke was billowing into the room from the left, from an adjacent room where the fire itself was located. A heated manikin lies on the floor in this scene, representing a victim. Vertical bar patterns on the back wall of this room were constructed from cooled pipes. The "Temp" and "BATTERY" indicators were added by the particular fire-fighter infrared camera that captured this original image. No attempt to remove them was made for the example described above, though in general for realistic testing of other fire-fighter cameras they would be removed from the projected imagery. As the video clip progresses, the room fills with smoke, and eventually the point is reached where the location of the manikin can no longer be identified. For high enough quality projected imagery, this point will depend on the image quality of the camera under test. Thus, an example application is for the projector to be used to reproducibly test which camera of several candidates can best see victims in smoke filled rooms – without requiring live fire testing.

4. MODULATION TRANSFER FUNCTION

The modulation transfer function (MTF) is one of the main parameters traditionally used by optical engineers to quantify the quality of an optical system. It is defined as the magnitude of the optical transfer function (OTF), or the magnitude response of the optical system to sinusoidal spatial patterns having different spatial frequencies. For optical systems in the range it is challenging produce reliable sinusoidal test patterns as physical artifacts. Thus an application for the projector described here is to produce virtually sinusoidal patterns for testing MTF of fire-fighter cameras. The goal here was to test the projection system with the configuration mentioned above and show that it can be good enough to project such targets to enable the MTF of the camera system to be determined. For now, the system MTF will be determined.

The experimental setup used for MTF measurements is the same as that used above, depicted in Fig. 9. Vertical sinusoidal patterns where displayed on the DMD after being converted to the micro-checker format and were projected into the camera. A total of 106 patterns where projected onto the screen, each at a different spatial frequency from zero up to the camera Nyquist limit (0.5 cycles/camera pixel). The spatial frequency increments where constant. The projector and camera ran asynchronously for this preliminary testing, so multiple frames were averaged to smooth out the resulting temporal artifacts. For this experiment fifty temporal frames per spatial frequency point where taken and averaged. The camera was calibrated for radiance during the same test session against a blackbody temperature set to 308.15 K. The camera integration time was set to 41 ms for all the MTF measurements and the for the blackbody calibration. Also fifty-frame averages were taken for each of the scenes "all-mirrors-on", "all-mirror-off", and background (laser or argon-arc source blocked). Figure 11 shows a typical sinusoidal and bar pattern images measured for the two different projection systems.
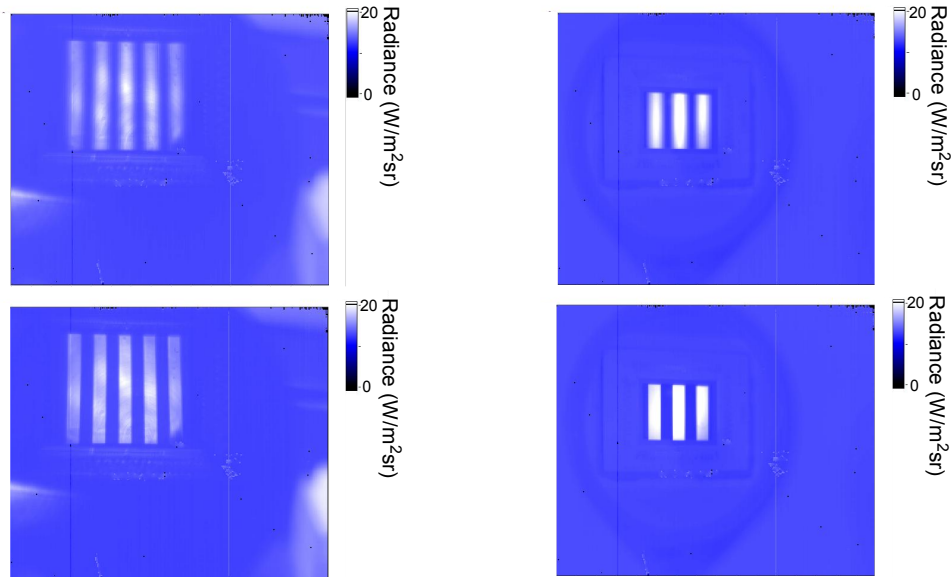
Figure 11. Typical images measured by the microbolometer camera during MTF measurements of the projectors. CO_2 laser based indirect projection is shown on the left. Argon-arc source based direct projection is on the on the right. The top images are sinusoidal patterns and the bottom images are bar patterns.
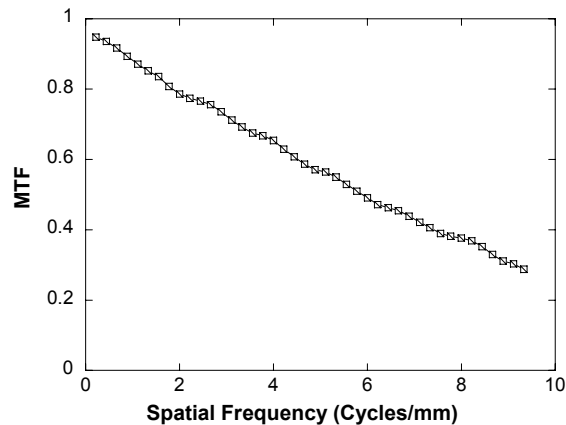

Figure 12. Result of system modulation transfer function measurements referred using the direct-projection method to project sinusoidal patterns displayed on the MAPS DMD with a magnification of 0.27 onto the focal plane of the microbolometer camera.

The system MTF was found for the condition where the magnification $M = 0.27$ (Fig. 12), meaning that the DMD was demagnified by a factor of about three by the projection optics. The footprint frequency cutoff of the DMD projected onto the camera focal plane is equal to $1/Mw$, where w is the DMD pixel width, 34 μm for the micro-checkers scheme. Thus the DMD footprint MTF cutoff is 109 cycles/mm. The camera pixel pitch is $w_c = 50$ μm, so the camera footprint cutoff is $1/w_c = 20$ cycles/mm. This means that with this arrangement the DMD projection has enough resolution to test the camera and its optics.

The contract ratio C at low spatial frequency was computed as from the bar patterns as

$$C = \frac{L_{on} - L_{background}}{L_{off} - L_{background}},$$ (3)

where L_{on}, L_{off}, and $L_{background}$ were computed from the bar pattern images as the average radiance for regions associated with on DMD pixels, off DMD pixels, and background, respectively. For the CO_2 laser projection system we measured a contrast ratio of 16 ± 3 (k=1). For the argon-arc direct projection system, we measured a contrast ratio of 75 ± 4 (k=1), with a maximum apparent temperature of about 360 K ± 2 K (k=1). Note that we have not tried yet to optimize these projectors yet for maximum apparent temperature.

5. SUMMARY

We have discussed preliminary results on developing a infrared scene projector for testing fire-fighter infrared cameras, both with realistic imagery and with sinusoidal and bar patterns. Diffraction characterization measurements of the DMD provided insight on projection schemes that increase brightness and contrast. Initial images of real fire testing scenes projected and captured with a laboratory microbolometer camera look promising, and initial MTF measurements were performed that were limited by the optics.

ACKNOWLEDGEMENT

[*]Note: References are made to certain commercially available products in this paper to adequately specify the experimental procedures involved. Such identification does not imply recommendation or endorsement by the National Institute of Standards and Technology, nor does it imply that these products are the best for the purpose specified.
DMD is a trademark of Texas Instruments, Inc.

REFERENCES

1. Woodworth, S. P., "Choosing a thermal imaging unit," *Fire Engineering* **153** (1), 83-84 (2000).
2. "Proposed NFPA 1801 Standard on Thermal Imagers for the Fire Service, 2009 Edition," National Fire Protection Association, September 2007.
3. ASTM E 1543-00, "Standard test method for noise equivalent temperature difference of thermal imaging systems," ASTM International, West Conshohoken, PA (2000).
4. D. B. Beasley, M. Bender, J. Crosby, T. Messer, and D. A. Saylor, "Dynamic IR scene projector based upon the digital micromirror device," *Proc. SPIE* **4366**, 96-102 (2001).
5. D. B. Beasley, D. A. Saylor and J. Buford, "Overview of dynamic scene projectors at the U. S. Army Aviation and Missile Command," *Proc. SPIE* **4717**, 136-147 (2002).
6. D. B. Beasley, M. Bender, J. Crosby, T. Messer, and D. A. Saylor, "Advancements in the micromirror array projector technology," *Proc. SPIE* **5092**, 71-82 (2003).
7. W. R. Folks, D. Mullally, G. Zummo, A. Weeks, and G. Boreman, "DMD-based infrared scene projection: a comparison of MWIR and LWIR modulation transfer function," *Proc. SPIE* **5408**, 199-202 (2004).
8. W. R. Folks, J. M. López-Alonso, B. Monacelli, A. Weeks, G. Zummo, D. Mullally, and G. Boreman, "Characterization of a digital-micromirror device-based infrared scene projector," *Opt. Eng.* **44**, pp-pp (2005).
9. W. Duncan, B. Lee, P. Rancuret, B. Sawyers, W. Stalcup, L. Endsley, and D. Powell, "DLP switched blaze grating: the heart of optical signal processing," *Proc. SPIE* **4983**, 297-304 (2003).
10. M. H. Hutley, Diffraction Gratings (Academic Press, New York, 1982), pp. 36-38.
11. D. C. O'Shea, Elements of Modern Optical Design (Wiley, New York, 1985), pp. 327-328.
12. J. M. Bridges and A. L. Migdall, "Characterization of argon arc source in the infrared," *Metrologia* **32**, 625-628 (1996/96).
13. G. D. Boreman, Modulation Transfer Function in Optical and Electro-Optical Systems, (SPIE Press, Bellingham, 2001).